



Electric potential differences across auroral generator interfaces

J. De Keyser and M. Echim

Belgian Institute for Space Aeronomy (BIRA-IASB), Ringlaan 3, 1180 Brussels, Belgium

Correspondence to: J. De Keyser (johan.dekeyser@aeronomie.be)

Received: 8 November 2012 – Revised: 19 December 2012 – Accepted: 20 January 2013 – Published: 19 February 2013

Abstract. Strong localized high-altitude auroral electric fields, such as those observed by Cluster, are often associated with magnetospheric interfaces. The type of high-altitude electric field profile (monopolar, bipolar, or more complicated) depends on the properties of the plasmas on either side of the interface, as well as on the total electric potential difference across the structure. The present paper explores the role of this cross-field electric potential difference in the situation where the interface is a tangential discontinuity. A self-consistent Vlasov description is used to determine the equilibrium configuration for different values of the transverse potential difference. A major observation is that there exist limits to the potential difference, beyond which no equilibrium configuration of the interface can be sustained. It is further demonstrated how the plasma densities and temperatures affect the type of electric field profile in the transition, with monopolar electric fields appearing primarily when the temperature contrast is large. These findings strongly support the observed association of monopolar fields with the plasma sheet boundary. The role of shear flow tangent to the interface is also examined.

Keywords. Magnetospheric physics (Auroral phenomena; Plasma sheet) – Space plasma physics (Discontinuities)

1 Introduction

Cluster surveys of high-altitude auroral electric fields have consistently shown that intense localized electric fields are found at magnetospheric plasma boundaries above the auroral acceleration region (Johansson et al., 2005, 2006). Such fields play a key role in the auroral current system. The observed electric field profiles have been classified into “convergent” and “divergent” electric fields (e.g. Lyons, 1980, 1981; De Keyser and Echim, 2010), or into “monopolar” and “bipolar” fields (e.g. Johansson et al., 2006; De Keyser et al.,

2010, 2011). The Cluster observations indicate an association of monopolar fields with the lobe–plasma sheet interface (mapping onto the polar cap boundary), and of bipolar electric fields with interfaces within the plasma sheet (mapping inside the oval).

Auroral interfaces are typically field-aligned, with a strong and almost unidirectional magnetic field. Minor magnetic field variations are produced by the field-aligned currents that connect magnetosphere and ionosphere, and are superimposed on the background geomagnetic field. Additional magnetic field variations may be due to waves. We will consider the limit case in which the interface is a quasi-steady structure that is exactly parallel to the magnetic field; that is, the interface has an equilibrium tangential discontinuity configuration (TD).

The structure of TD interfaces has been studied in great detail in the past (see the review by Roth et al., 1996, and references therein). In a one-dimensional planar TD configuration, all particle guiding centers move parallel to the interface. How the particles arrive at a specific position in the structure in the first place is a question known as the “accessibility problem” (Whipple et al., 1984). Using reasonable assumptions, a realistic set of particle velocity distributions can be put forward based on only a few parameters. The Vlasov–Maxwell equations must then be solved, as the Vlasov equations expressing the conservation of particles in phase space and Maxwell’s laws impose constraints on the allowed plasma and field configurations. Solving the Vlasov–Maxwell equations in this fully kinetic description is fairly easy (Roth et al., 1996).

The nature of a tangential discontinuity boundary strongly depends on the boundary conditions, in particular on the total electric potential across the layer and/or the flow shear (e.g. Sestero, 1964, 1966). An external electric potential difference (EPPD) between the two plasmas enforces the existence of an electric field perpendicular to the interface. Shear flows

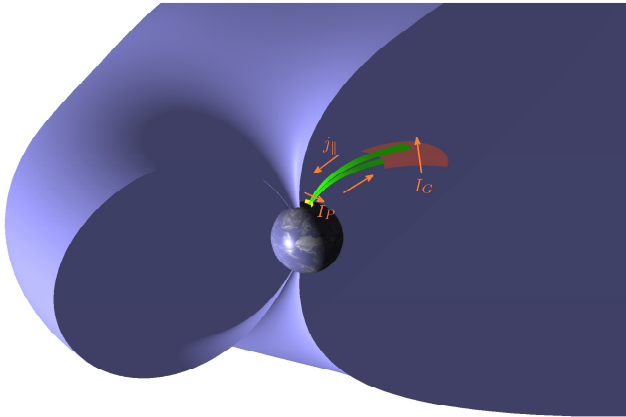


Fig. 1. A magnetospheric interface (brown) connects via field-aligned currents j_{\parallel} to the ionosphere, where the current system is closed by an ionospheric current (Pedersen current I_P). The driver is a generator current I_G across the interface.

are related to a corresponding convection electric field, also in the normal direction. As the temperatures of the plasma components and hence their gyroradii are different, they will react to this electric field differently, which provokes charge separation. This, in turn, produces a polarization electric field that counteracts the charge separation.

The present paper examines the role of the EEPD and of flow shear across a planar TD interface, for different plasma densities and temperatures that correspond to possible auroral configurations. De Keyser et al. (2010) presented a few typical TD configurations and concluded that interfaces between hot and cold plasmas, across which a significant EEPD is applied, give rise to monopolar electric fields. They are thus able to explain the association between monopolar fields and the lobe–plasma sheet boundary. This argument is explored here in further detail by conducting a more systematic survey of the effect of the EEPD on TD structure.

This paper is organized as follows. Section 2 presents the general plasma and field configuration. The TD model is briefly described in Sect. 3. Section 4 explains the basic structure of the equilibrium TD configuration of a typical auroral interface. Section 5 explores the effect of the EEPD on the structure of such auroral interfaces. How this effect is modulated by the plasma densities and temperatures is discussed in Sect. 6. Section 7 addresses the effects of shear flow. The paper concludes with a discussion of the consequences of these results for auroral current systems.

2 Plasma and field configuration

At the outset, it is assumed that the magnetosphere harbours sufficiently long-lived electric potential structures that drive auroral current systems: the quasi-electrostatic picture then applies (e.g. Lyons, 1980, 1981; Roth et al., 1993; De Keyser, 1999; Echim et al., 2008; De Keyser and Echim, 2010). Such

magnetospheric potential structures can act as generators and are connected via field-aligned currents j_{\parallel} to the ionosphere, where a horizontal current (the height-integrated Pedersen current I_P) closes the circuit, as sketched in Fig. 1; a current I_G must therefore exist across the magnetospheric interface. In other situations the ionosphere might be the driver while the magnetospheric interface behaves as a load. In either case, the interface cannot be a TD in the strict sense of the word, since there can be no plasma flow and hence no current across a TD interface. However, since the interface surface is very large, an extremely small current density across the interface suffices to balance the field-aligned currents that flow in thin sheets to and from the ionosphere, so that the interface may still be modelled as a TD, at least in a first approximation.

The present paper focuses on the situation in which the interface behaves as a generator. This generator can be long-lived only if the feedback effects in the auroral system are not too strong. This implies that particles lost to the ionosphere are replenished in the generator, so that the system remains in a quasi-static state. The interface might actually be a TD in which a certain amount of wave–particle scattering is able to compensate for this loss, or it might be a rotational discontinuity with a small normal component through which particles continuously access the interface layer, or convection along the boundary may replenish the loss cone, or the interface layer might itself be so large that it constitutes a reservoir of particles able to maintain the configuration for a sufficiently long time (several minutes, see lifetime estimates in Roth et al., 1993; De Keyser, 1999). The lifetime obviously depends on the intensity of the field-aligned currents. For low ionospheric conductivities the required currents can be quite weak and the lifetime correspondingly longer. Also, the contribution of ionospheric outflow is ignored in this study. The quasi-static assumption is believed to be appropriate at least for larger-scale auroral structures.

Another assumption is that the TD interface has a planar geometry. The overall surface radius of curvature is often on the scale of the magnetosphere ($R > 1 R_E$) while the interface thickness is of the order of the gyroradius of the hottest ions involved ($D < 600$ km for typical plasma sheet ion temperatures and magnetic field strength), so that this condition is satisfied ($D/R < 10\%$). When magnetohydrodynamic waves are present, however, deviations from planarity are likely important (De Keyser et al., 2011).

Auroral generator interfaces may be found in various places in the magnetosphere; the focus here is on interfaces involving the lobes and the plasma sheet. Such interfaces can be classified into two types: cold–hot interfaces, typical of the lobe–plasma sheet interface, and hot–hot interfaces, typical of substructure inside the plasma sheet. The magnetospheric lobes are populated with cold plasma. Because of its low temperature (a few eV at most), this plasma has often escaped detection. The lobe densities are believed to be $0.1\text{--}0.5\text{ cm}^{-3}$ (Engwall et al., 2006). The central plasma sheet is

more dense, up to a few particles per cm^3 , and much hotter, with ion energies of 5–20 keV. There is no reason why the electric potential on either side of the lobe–plasma sheet boundary, or of interfaces inside the plasma sheet, should be identical. The electric potential differences in the tail and across the plasma sheet are the result of the solar wind–magnetosphere coupling. This coupling may induce potential differences on the order of several tens of kV; the cross-tail potential, typically 40 kV (Haaland et al., 2008), is an example. There may also be shear flows across such interfaces, for instance, when bursty bulk flows are present with speeds of up to hundreds of km s^{-1} (Angelopoulos et al., 1992).

3 The TD model

The self-consistent kinetic TD model used here is the one discussed by Roth et al. (1996). We briefly describe its main features; the interested reader is referred to that reference for a more thorough discussion.

The constants of motion of a particle of species s with charge $Z_s e$ and mass m_s in an infinite planar TD layer are its energy and its canonical momenta (the x -axis is defined along the interface normal):

$$H = \frac{1}{2} m_s v^2 + Z_s e \phi, \tag{1}$$

$$p_y = m_s v_y + Z_s e A_y, \tag{2}$$

$$p_z = m_s v_z + Z_s e A_z, \tag{3}$$

where the electromagnetic field configuration is given by the scalar electric potential $\phi(x)$ and the magnetic vector potential $\mathbf{A} = [0, A_y(x), A_z(x)]$. If a particle in this 1-dimensional TD configuration has a gyroradius that is much smaller than the length scales over which ϕ and \mathbf{A} change (that is, the particle sees essentially zero electric field and a constant magnetic field), it simply gyrates around a magnetic field line in a helical orbit. If there is an electric field, or if there is a magnetic field gradient, the particle will experience the well-known electric or gradient-B drift parallel to the plane of the TD. While the particle orbits may be much more complicated than helical trajectories around field lines, it is easy to see that the particle will always move in a limited range in x , although it can drift along y and z . In this sense, each particle in a static TD configuration is “trapped”, as it always stays at essentially the same average position relative to the layer.

A consequence of the above is that many TD configurations are possible, although there are limitations. First, one has to respect the pressure balance condition that states that the total pressure,

$$P_{\text{tot}} = P_{\text{kin}}(x) + P_{\text{mag}}(x) = \sum_s n_s(x) k_B T_s(x) + \frac{B^2(x)}{2\mu_0}, \tag{4}$$

must be constant across the structure (k_B denotes Boltzmann’s constant). Second, one should try to avoid a strong

charge imbalance since that would provoke intense localized electric fields, and such configurations are not stable. Nevertheless, an infinite number of configurations remains possible. As Whipple et al. (1984) have pointed out, this indeterminacy can only be resolved by considering the mechanisms by which particles enter the TD layer, but that falls outside the scope of a stationary planar TD model.

In building a TD model, one therefore has to make a choice and pick “reasonable” particle distributions. We consider here a type of distribution that satisfies quite natural requirements: (a) far from the TD, the distribution is a Maxwellian; (b) at each position, the distribution has a single maximum in p_y, p_z space; (c) the distribution changes smoothly across the transition in p_y, p_z space. Such a reasonable choice is the following. Let $f_s(H, p_y, p_z)$ be the velocity distribution function (VDF) that describes a population s on the left side of the discontinuity. This VDF is chosen to be a Maxwellian with isotropic temperature T_s and a mean velocity \mathbf{V}_s for $x \rightarrow -\infty$,

$$F_s(H, p_y, p_z) = N_s \left(\frac{m_s}{2\pi k_B T_s} \right)^{\frac{3}{2}} e^{-\frac{H + \frac{1}{2} m_s V_s^2 - p_y V_{sy} - p_z V_{sz}}{k_B T_s}},$$

where N_s is a normalization constant that is proportional to the number density. Inside the discontinuity layer, this VDF typically will not remain Maxwellian. And on the other side of the discontinuity, for positive x , this VDF must vanish if the TD is to form a boundary separating different populations. This kind of argument must hold for all species (positively or negatively charged, to the left or the right of the TD boundary). In general, this requires some sort of “cutoff” in the distribution function that forces f_s to vanish on the opposite side of the TD. The VDF is therefore written as

$$f_s(H, p_y, p_z) = C_s(p_y, p_z) F_s(H, p_y, p_z) \tag{5}$$

with the cutoff function C_s satisfying

$$\lim_{x \rightarrow -\infty} C_s(p_y, p_z) = 1, \quad \lim_{x \rightarrow +\infty} C_s(p_y, p_z) = 0,$$

for a population on the left, and the converse for a population on the right. While the cutoff function operates in phase space, it results in a cutoff in geometrical space as well: it effectively forces the density on the other side of the TD to vanish. It is, in fact, the choice of the cutoff function that resolves the indeterminacy mentioned earlier. The cutoff function that is used here is essentially that of Roth et al. (1996), although the formulation is slightly different. This choice is a generalization of earlier theoretical descriptions of TD structure (Sestero, 1964, 1966; Lemaire and Burlaga, 1976; Lee and Kan, 1979). Let θ_s be an angle in the y, z -plane somewhere in between the asymptotic magnetic field clock angles θ_{left} and θ_{right} on either side. Rotate (y, z) and (p_y, p_z) over angle θ to (y', z') and $(p_{y'}, p_{z'})$. In the rotated frame the y' -axis is oriented in between the magnetic field directions on

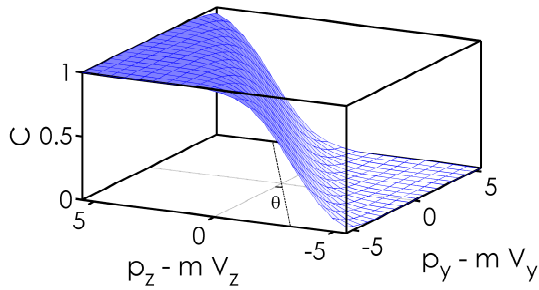


Fig. 2. The cutoff function in phase space is an important ingredient in tangential discontinuity models, as it ensures that a population is present on only one side of the TD interface. The plot illustrates the cutoff function for a transition length $\ell = 2$ and an orientation of the cutoff line (where $C = 1/2$) given by $\theta = 30^\circ$.

either side. One can then define the cutoff function as

$$C_s(p_y, p_z) = [\alpha_s \operatorname{erfc}(-U_s) + (1 - \alpha_s) \operatorname{erfc}(+U_s)]/2$$

$$U_s = \frac{p_z' - m V_{sz'}}{\operatorname{sign}(Z_s) \sqrt{2m_s k_B T_s (\ell_s^2 - 1)}},$$

where α_s is 0 or 1, depending on whether the population is on the left or on the right side. The dimensionless free parameter $\ell_s \geq 1$ determines the sharpness of the cutoff. The cutoff function is graphically represented in Fig. 2, where the angle θ_s gives the orientation of the cutoff line in the p_y, p_z -plane and ℓ_s determines the thickness of the transition zone. For $\ell_s \rightarrow 1$, the cutoff in phase space has zero thickness, while for larger values a smoother transition is obtained. It can be shown that ℓ_s can be regarded as a dimensionless length scale, since the characteristic transition length of a population is $L_s = \ell_s \rho_s$, with $\rho_s = \sqrt{2m_s k_B T_s} / |Z_s| e B$ the gyroradius of a thermal particle of species s and temperature T_s in a magnetic field of strength B .

An interesting property of this particular form of VDFs is that its moments

$$Q_s^{(ijk)} = \int \int \int v_x^i v_y^j v_z^k f_s(v_x, v_y, v_z) dv_x dv_y dv_z$$

can be computed analytically (see Roth et al., 1996, Appendix A). Consequently, the partial densities $n_s = Q_s^{(000)}$ and currents $j_{sy} = Z_s e Q_s^{(010)}$ and $j_{sz} = Z_s e Q_s^{(001)}$ can be expressed in terms of the potentials ϕ and A . The time-stationary Maxwell equations can then be formulated as

$$\frac{dA_y}{dx} = +B_z(x), \quad (6)$$

$$\frac{dA_z}{dx} = -B_y(x), \quad (7)$$

$$\frac{dB_y}{dx} = +\mu_0 \sum_s j_{sz}(\phi(x), A_y(x), A_z(x)), \quad (8)$$

$$\frac{dB_z}{dx} = -\mu_0 \sum_s j_{sy}(\phi(x), A_y(x), A_z(x)), \quad (9)$$

$$0 = \sum_s Z_s n_s(\phi(x), A_y(x), A_z(x)), \quad (10)$$

where the last equation expresses quasi-neutrality and replaces the Poisson equation. This system of equations is a nonlinear differential algebraic problem. Given B_y, B_z, A_y, A_z , and ϕ at a point x_0 , the solution can be obtained by step-wise integration of the four ordinary differential Eqs. (6)–(9) and by iterative solution of the implicit nonlinear algebraic Eq. (10) at each step. Because of the various length scales that may be involved, the use of a variable step integrator is advised.

Once the electromagnetic potentials ϕ and A are computed from Maxwell's equations, the conserved quantities are known so that the VDFs and their moments are obtained throughout the TD layer, since the dependency of the VDFs on H, p_y , and p_z is fixed and since these are conserved quantities. One therefore has found a steady-state planar TD configuration. Note, however, that this solution depends on the choice of the cutoff, and in particular of the dimensionless transition lengths ℓ_s . This solution also depends on the boundary conditions that are supplied (the magnetic field orientations θ_{left} and θ_{right} , and the external electric potential difference $\Delta\phi_{\text{ext}}$). Nothing is known a priori about the possible stability of the configuration.

Given the arbitrariness in the choice of distribution functions, it is advisable to verify whether this TD model is realistic. To that end, this model has been confronted with observations of solar wind discontinuities (De Keyser et al., 1996, 1997), of the magnetopause (Hubert et al., 1998; Echim et al., 2011), and of auroral generator interfaces (Echim et al., 2009). In all these situations, a good agreement between model and observations was obtained, suggesting that the choice of distribution functions is an appropriate one.

4 Equilibrium configuration of auroral interfaces

In this section the TD model is applied to a typical cold-hot (lobe-plasma sheet) and hot-hot (plasma sheet-plasma sheet) interface, and the importance of the characteristic lengths is discussed.

The simplest TD is one where the interface separates two different stationary proton-electron plasmas. Consider an interface between a cold lobe plasma with a density of 0.1 cm^{-3} , consisting of 1 eV electrons and 5 eV protons, and a hot plasma with a typical plasma sheet density of 0.5 cm^{-3} , consisting of 1 keV electrons and 5 keV protons. We have chosen an ion-to-electron temperature ratio of 5, which is well established for the plasma sheet but less known for the lobe; the precise temperature ratio actually does not matter much for the analysis presented here. The magnetic field at the center ($x = 0$) is taken to be 40 nT, with the field oriented along the z -axis. For the moment, it is assumed that the plasma populations on either side have zero mean velocity and that there is no net electric potential difference across the structure.

The thermal gyroradii of these distributions are $\rho_{\text{cold}-} = 0.084\text{km}$, $\rho_{\text{cold}+} = 8.0\text{km}$, $\rho_{\text{hot}-} = 2.7\text{km}$, and $\rho_{\text{hot}+} = 256\text{km}$. Because of the large proton-to-electron mass ratio, and also due to the temperature differences, the ion and electron gyroradii are quite different. The transition length scales of the four populations, however, should not be too disparate since that would give rise to very strong localized charge-separation electric fields that are likely to render the structure unstable. Physical considerations suggest that $\rho_+ \leq L_+ < 5\rho_+$ and $1 < L_+/L_- < 10$; this is achieved here with the choice $\ell_+ = \ell = 1$ and $\ell_- = 40\ell = 40$ so that the transition lengths are ordered from small to large as $L_{\text{cold}-} = 3.4\text{km} < L_{\text{cold}+} = 8.0\text{km} \ll L_{\text{hot}-} = 108\text{km} < L_{\text{hot}+} = 256\text{km}$.

Consider a configuration where the magnetic field is unidirectional along z , i.e. $\theta_{\text{left}} = \theta_{\text{right}} = 90^\circ$. Because the plasma beta is fairly low ($\beta < 1.2$), the magnetic field strength does not change much. The cutoff direction is chosen as $\theta_s = 90^\circ$ for all populations, so that in the rotated frame $B_{y'} > 0$ and $\lim_{x \rightarrow \pm\infty} A_{z'}(x) \approx \mp\infty$. Hence, $\lim_{x \rightarrow \pm\infty} p_{z'} = \text{sign}(-Z_s) \lim_{x \rightarrow \pm\infty} A_{z'} = \text{sign}(\pm Z_s) \cdot \infty$, and $\lim_{x \rightarrow \pm\infty} U_s(x) = \pm\infty$. By choosing $\alpha_s = 0$ or 1 , the cutoff will act to limit the population to the $x < 0$ or $x > 0$ side respectively.

Figure 3a shows the equilibrium configuration for the cold-hot interface. The computations have been performed for three different choices of characteristic lengths: $\ell = 1, 2$, and 3 , corresponding to $\ell_+ = 1, 2, 3$ and $\ell_- = 40, 80, 120$. One readily observes, for $\ell = 1$, that the half-width of the transition as visible in the variation of B_z is about 250km , which corresponds to the hot ion gyroradius $L_{\text{hot}+}$. The layer widens for larger ℓ . The hot particle densities across the TD (red and blue curves in the third panel of Fig. 3a) vary on the different length scales $L_{\text{hot}-}$ and $L_{\text{hot}+}$. This produces a polarization electric field over a distance on the order of $L_{\text{hot}+}$, which is rather large. The cold ions and electrons (grey and green curves) create a similar charge separation effect, but the polarization electric field exists only over a distance of about $L_{\text{cold}+}$; this is much shorter. Since there is no external electric potential difference, there is a broad region (thickness scale $L_{\text{hot}+}$) with a small electric field $|E_x|$ and a narrow region (thickness scale $L_{\text{hot}-}$) with a large $|E_x|$ in the opposite sense, so that

$$\Delta\phi_{\text{ext}} = - \int_{-\infty}^{+\infty} E_x dx = 0.$$

Hence, the positive and negative electric field excursions are asymmetric. The polarization electric field can be up to several mV m^{-1} . Its strength is roughly inversely proportional to the width of the layer ($E_{x,\text{max}} \propto 1/\ell$).

Figure 3b shows the equilibrium configuration for a typical hot-hot interface. The overall thickness of the layer is of the same order as for the cold-hot interface, since the maximum characteristic length scale is $L_{\text{hot}+}$ in both cases. Since the

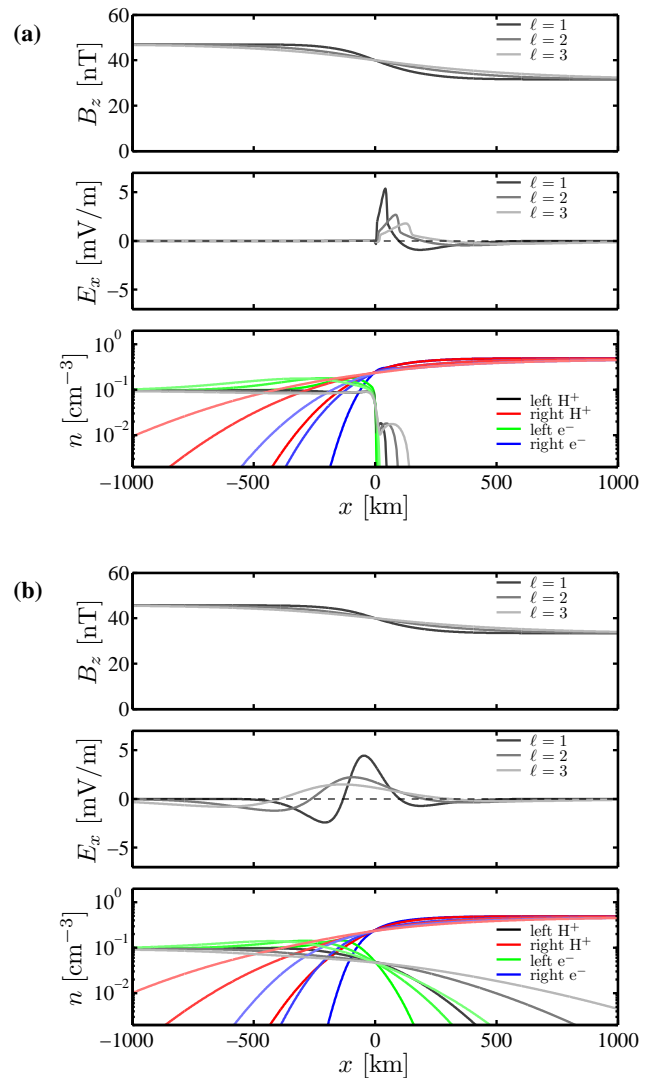


Fig. 3. Structure of a tangential discontinuity for (a) a cold-hot plasma interface between a 1eV electron and 5eV proton plasma with density 0.1cm^{-3} on the left side and a 1keV electron and 5keV proton plasma with density 0.5cm^{-3} on the right, and (b) a hot-hot plasma interface between two 1keV electron and 5keV proton plasmas with densities 0.1cm^{-3} on the left side and 1cm^{-3} on the right. The top panels show the magnetic field profile across the structure (B_z component; the field is unidirectional along z), the middle panels give the electric field, and the bottom panels plot the densities of the four plasma populations involved. The solutions are obtained for zero external electric potential difference across the discontinuity and in the absence of flow shear. The computations have been carried out for dimensionless transition lengths $\ell = \ell_+ = 1, 2, 3$ and the corresponding values $\ell_- = 40, 80, 120$.

plasmas on either side of the hot-hot interface have the same temperatures, there are only two length scales that play a role. The electric field profile is less asymmetric; it is solely due to the density difference between the two sides. Again the relation $E_{x,\text{max}} \propto 1/\ell$ seems to hold.

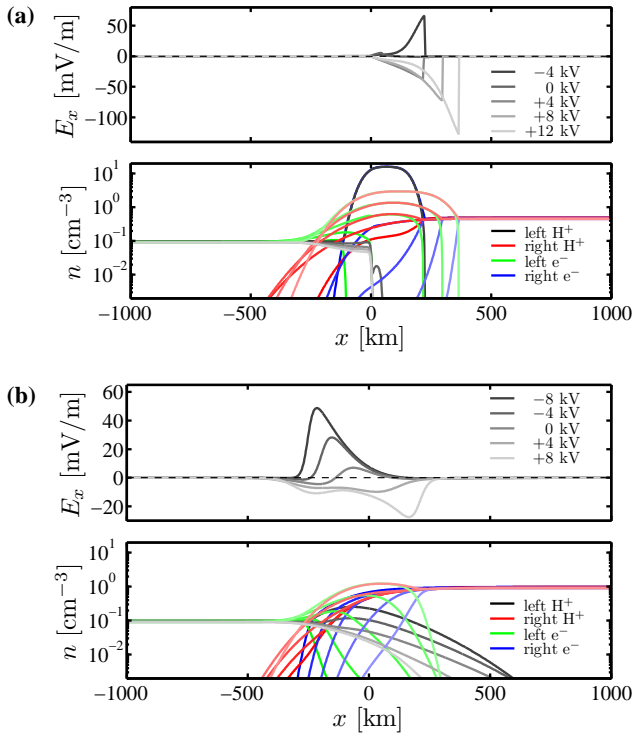


Fig. 4. Structure of a tangential discontinuity for (a) a cold-hot plasma interface and (b) a hot-hot plasma interface; the properties of the cold and hot plasmas are the same as in Fig. 3. The top panels show the electric field profile and the bottom panels plot the densities of the four plasma populations involved. The dimensionless transition lengths are $\ell_+ = 1$ and $\ell_- = 40$. The solutions are shown for various values of the external electric potential difference and in the absence of flow shear.

The interface becomes wider and the electric field correspondingly weaker for larger transition lengths, but the interface structure does not change qualitatively. That is why, in the remainder of this paper, mostly the choice $\ell = 1$ is used.

5 Role of external electric potential difference

In this section, the role of an external electric potential difference $\Delta\phi_{\text{ext}}$ is examined. This is a boundary condition that is imposed while solving the differential algebraic system in Eqs. (6)–(10). The presence of such an EEPD modifies the electric field structure inside the transition, and it therefore has an important effect on the resulting configuration.

The electric structure of the same cold-hot TD interface as before (for $\ell = 1$) has been computed for various values of the EEPD. Figure 4a summarizes the results. A first observation is that the electric field profiles that are obtained (for significant values of $\Delta\phi_{\text{ext}}$) are monopolar, with field strengths up to several tens of mV m^{-1} and with a polarity determined by the sign of $\Delta\phi_{\text{ext}}$. Comparing the solution for $\Delta\phi_{\text{ext}} = -4\text{ kV} < 0$ with that for zero EEPD, it is seen that

the external potential attracts hot electrons to the center of the layer and repels the hot protons, while it does the reverse for the cold plasma species. The converse is true when $\Delta\phi_{\text{ext}} > 0$. For the hot-hot interface (also for $\ell = 1$), electric field profiles are obtained that may have a bipolar or a more complicated character as long as $\Delta\phi_{\text{ext}}$ is small, but that also become monopolar for larger EEPD (Fig. 4b). The detailed profiles depend on the density asymmetry and on the temperatures.

The behaviour of a TD in response to an external electric potential difference can be understood in terms of the following simple argument. The TD thickness can be roughly approximated as $L \approx L_{\text{hot}+}$ for monopolar fields and $L \approx 2L_{\text{hot}+}$ for bipolar fields, as the hot ions have the biggest transition length. Making abstraction of the polarization electric field (which can only be done when considering the hot ions, with the largest spatial scale), the average electric field in the layer due to an external electric potential difference $\Delta\phi_{\text{ext}}$ must be

$$E_{\text{ext}} \approx -\frac{\Delta\phi_{\text{ext}}}{L}. \quad (11)$$

Since L scales with ℓ , this explains the inverse proportionality between $E_{x,\text{max}}$ and ℓ observed earlier. A particle with charge $Z_{\text{hot}+}e$ and perpendicular thermal velocity $v_{\text{hot}+\perp}$ inside the layer then experiences a Lorentz force associated with its gyrating motion in the ambient magnetic field with strength B as well as the electric force due to the EEPD. If the Lorentz force is stronger than the external electric field, $v_{\text{hot}+\perp}B > |E_{\text{ext}}|$, an equilibrium configuration is possible. If not, the electric field is so strong that the Lorentz force cannot tie the particles to the field lines and no equilibrium is possible. An equilibrium can be found as long as

$$\Delta\phi_{\text{ext}} < \Delta\phi_{\text{TDmax}} = v_{\text{hot}+\perp}BL, \quad (12)$$

where $\Delta\phi_{\text{TDmax}}$ is a rough upper limit to the maximum EEPD for which a TD equilibrium can exist. Since $L_{\text{hot}+} = \ell\rho_{\text{hot}+} = \ell m_+ v_{\text{hot}+\perp} / Z_{\text{hot}+}eB$, this condition can be written for monopolar fields as

$$\Delta\phi_{\text{ext}} < \Delta\phi_{\text{TDmax,monopolar}} = \frac{2\ell W_{\text{hot}+\perp}}{Z_{\text{hot}+}e}, \quad (13)$$

with $W_{\text{hot}+\perp}$ the hot ion energy, and for bipolar fields as

$$\Delta\phi_{\text{ext}} < \Delta\phi_{\text{TDmax,bipolar}} = \frac{4\ell W_{\text{hot}+\perp}}{Z_{\text{hot}+}e}. \quad (14)$$

These expressions are similar to the velocity limit that has been deduced analytically for the analogous case of an external flow shear across the TD (but with $\Delta\phi_{\text{ext}} = 0$) by De Keyser et al. (1997).

It should be noted that, even for EEPD below the limits given by Eqs. (13)–(14), instabilities may occur that further restrict the possible TD configurations.

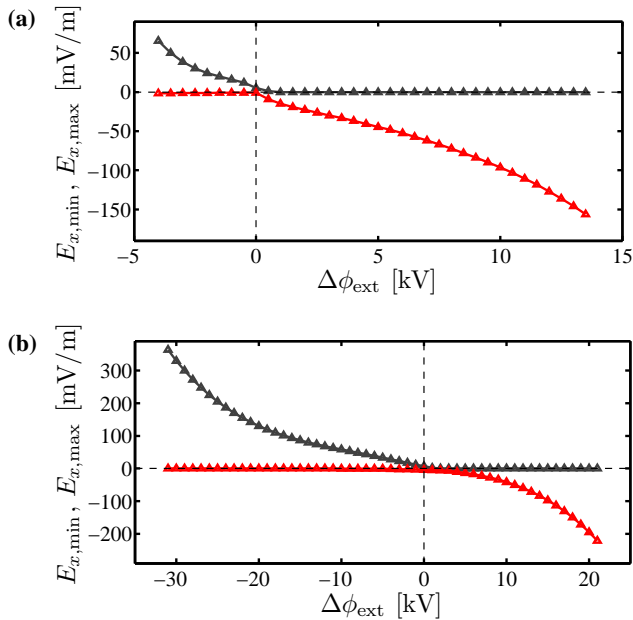


Fig. 5. Maximum (black) and minimum (red) electric field values in (a) a cold-hot tangential discontinuity and (b) a hot-hot discontinuity (see caption of Fig. 3) as a function of external electric potential difference. Both plots indicate the existence of upper and lower limits to the external potential difference for which an equilibrium can be found. Only for small $|\Delta\phi_{\text{ext}}|$ less than a few kV one finds $|E_{x,\text{max}}| \approx |E_{x,\text{min}}|$; the interfaces are characterized by a monopolar electric field signature elsewhere.

The above reasoning is only qualitative. We now verify the validity of the qualitative argument with the kinetic model that does include the effect of the polarization field. The TD model was used to compute the solutions for a range of $\Delta\phi_{\text{ext}}$ values. Figure 5 shows the minimum and maximum electric field values $E_{x,\text{min}} = \min_x E_x(x)$ and $E_{x,\text{max}} = \max_x E_x(x)$ as a function of $\Delta\phi_{\text{ext}}$ for the cold-hot and hot-hot interfaces. In either case, limits are found in the range of admitted EEPD values for which a TD equilibrium exists. The limits for cold-hot interfaces are found to be -4.2 kV and $+13.7\text{ kV}$. Equation (13) gives a maximum value $\Delta\phi_{\text{TDmax}}$ of 10 kV for 5 keV hot protons, which is indeed indicative of the observed upper limit. The EEPD limits for hot-hot TD interfaces are -31.5 kV and $+21.5\text{ kV}$, larger than the value of 20 kV obtained from Eq. (14). Such cross-field potential differences may actually be reached in the magnetotail.

Only for small $|\Delta\phi_{\text{ext}}|$, less than a kilovolt or so, the maxima and minima of the electric field profile are comparable ($|E_{x,\text{max}}| \approx |E_{x,\text{min}}|$). The fact that either $|E_{x,\text{max}}| \gg |E_{x,\text{min}}|$ or $|E_{x,\text{max}}| \ll |E_{x,\text{min}}|$ elsewhere demonstrates that cold-hot interfaces are nearly always characterized by a monopolar signature, while hot-hot interfaces also have monopolar fields as soon as $|\Delta\phi_{\text{ext}}|$ is larger than a few kV.

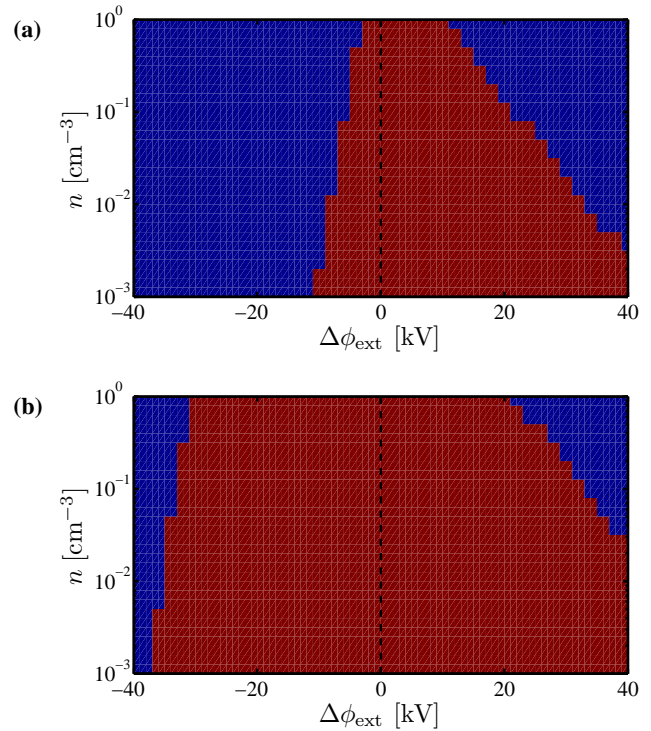


Fig. 6. Existence of a tangential discontinuity equilibrium between (a) cold and hot plasmas, with the cold plasma density being 0.1 cm^{-3} and the hot plasma density varying between 0.001 cm^{-3} and 1 cm^{-3} , and (b) two hot plasmas, with a density on the left side of 0.1 cm^{-3} and a density on the right side varying from 0.001 cm^{-3} to 1 cm^{-3} . In both cases the computations have been carried out over a broad range of EEPD values. The red regions indicate the existence of a tangential discontinuity; in the blue regions no tangential discontinuity equilibrium is possible.

6 Role of plasma properties

The above calculations illustrate the role of the plasma properties in determining the electric field profiles and the response to an external electric potential difference. This section therefore examines the effects of varying plasma densities and temperatures in combination with an EEPD on the existence of an equilibrium solution.

In order to determine for which TD configurations an equilibrium exists or not, a large set of model computations has been carried out. An automated routine determines whether an equilibrium solution can be found for the specified parameters. In practice, this implies checking whether the boundary conditions can be met and whether uniform asymptotic plasma states are obtained on either side of the boundary. Such an automatic test may deliver slightly different results depending on the numerical parameters with which the integration of the differential algebraic equations is carried out. Particular attention was therefore given to the size of the simulation domain (large enough to deal with configurations with very hot particles that have a large gyroradius), the

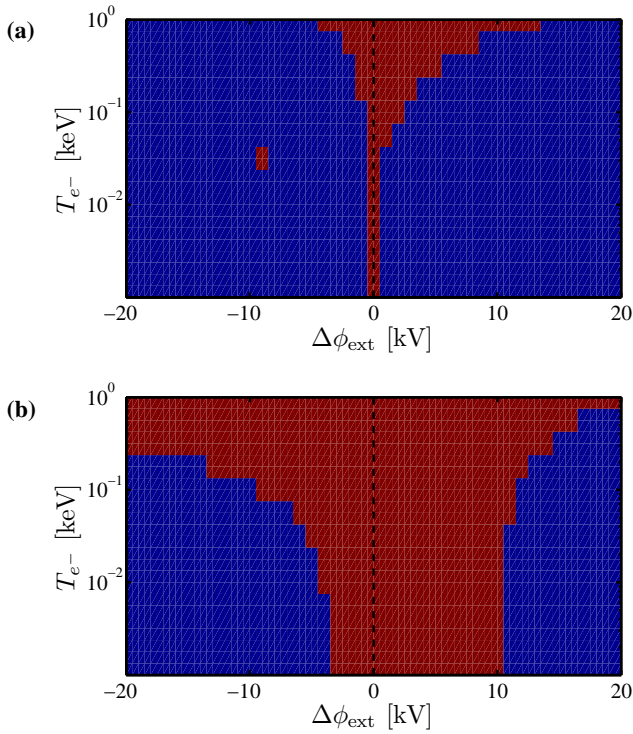


Fig. 7. Existence of a tangential discontinuity equilibrium between (a) plasmas of different temperatures, while the left density is 0.1 cm^{-3} and temperatures vary from $T_{e-} = 1 \text{ eV}$ up to 1 keV for the electrons and $T_{H+} = 5T_{e-}$ for the protons, while the right plasma consists of 1 keV electrons and 5 keV protons with a density of 0.5 cm^{-3} , and (b) two plasmas with the same temperatures, with left and right densities of 0.1 cm^{-3} and 0.5 cm^{-3} and with electron and ion temperatures varying through the same range as in panel (a). In both cases the computations have been carried out over a broad range of EEPD values. The red regions indicate the existence of a tangential discontinuity; in the blue regions no tangential discontinuity equilibrium is possible.

number of discretization points (large enough to resolve also the small length scales), the precision of the ordinary differential equation integrator and the solver for the nonlinear algebraic equation, etc.

Figure 6a reports the results of a number of simulations of the cold-hot plasma interface, in which the hot plasma density varies between 0.001 cm^{-3} and 1 cm^{-3} , and where $\Delta\phi_{\text{ext}}$ varies between -40 kV and $+40 \text{ kV}$. The red region represents the domain in parameter space where a TD equilibrium is found to exist. Figure 6b similarly plots the existence domain for a hot-hot interface where the right plasma density and the EEPD vary over the same range as before. Increasing the hot plasma density appears to lead to a more restricted range of $\Delta\phi_{\text{ext}}$. This can be understood as follows. The particles in the transition redistribute themselves to counter charge separation, but as they do so, the plasma pressure changes. Changes in the plasma pressure, however, are limited because of the requirement of constant total pressure

as expressed by Eq. (4). Particle redistribution is therefore easiest for low plasma beta, i.e. if the densities are smaller.

Existence domains for a tangential discontinuity equilibrium between plasmas with different or with the same temperatures are given in Fig. 7. The left density is 0.1 cm^{-3} , while the density on the right is 0.5 cm^{-3} . In the first panel, the left population temperatures vary from $T_{e-} = 1 \text{ eV}$ up to 1 keV for the electrons and $T_{H+} = 5T_{e-}$ for the protons, while the right plasma consists of 1 keV electrons and 5 keV protons. The structure of these transitions is determined by the ordering of the transition lengths. At the low temperature end $L_{\text{cold-}} < L_{\text{cold+}} < L_{\text{hot-}} < L_{\text{hot+}}$ and the precise $T_{\text{cold+}}/T_{\text{cold-}}$ ratio does not matter much. As the temperature increases, this ordering changes. At the high temperature end, the electron lengths are still shorter than the ion lengths so that the results are not qualitatively modified when the $T_{\text{cold+}}/T_{\text{cold-}}$ ratio is changed somewhat. In the second panel, both plasmas have the same temperatures, varying through the same ranges. Higher temperatures invariably lead to broader limits for $\Delta\phi_{\text{ext}}$: as the temperature increases, $\Delta\phi_{\text{TDmax}}$ increases as well.

7 Role of shear flow

The realization that the external electric potential difference places limits on the existence of TD equilibria is closely related to earlier work on the flow shear limit across a TD, since flow shear generates a potential difference across a finite-thickness TD layer (Sestero, 1964, 1966; Roth et al., 1996; De Keyser et al., 1997; De Keyser, 1999; Echim et al., 2007).

In that spirit, it is natural to examine the existence conditions when both a flow shear ΔV and an EEPD $\Delta\phi_{\text{ext}}$ are present. Figure 8 shows the existence domain for cold-hot interfaces with $\Delta\phi_{\text{ext}} = -2 \text{ kV}$, 0 kV , and $+2 \text{ kV}$ for $\ell = 1$. Note that the existence domain depends on the shape of the cutoff functions through the characteristic transition length values. The domains are symmetric with respect to the ΔV_{\parallel} axis. This can be explained by noting that the VDFs (where the mean velocities are $V_s = \pm\Delta V/2$ with the sign indicating on which side the population is located) are insensitive to a change of the sign of ΔV_{\parallel} as it does not appear in the cutoff function in the unidirectional magnetic field configuration considered here. The sense of ΔV_{\perp} , however, is important since it determines the sign of the convection electric field. If the EEPD-related field has the same sign, the two tend to reinforce each other. If they have opposite signs, they may partially cancel. In either case the degree of charge-separation is affected, and thus the existence condition will be modified. Even for the relatively small $\Delta\phi_{\text{ext}}$ examined in these simulations, the existence domain is modified significantly. For the hot-hot interface (not shown in Fig. 8), the shear velocity limits are higher because of the larger thermal velocities of the populations involved, so that the velocity limits likely play a lesser role in the magnetotail.

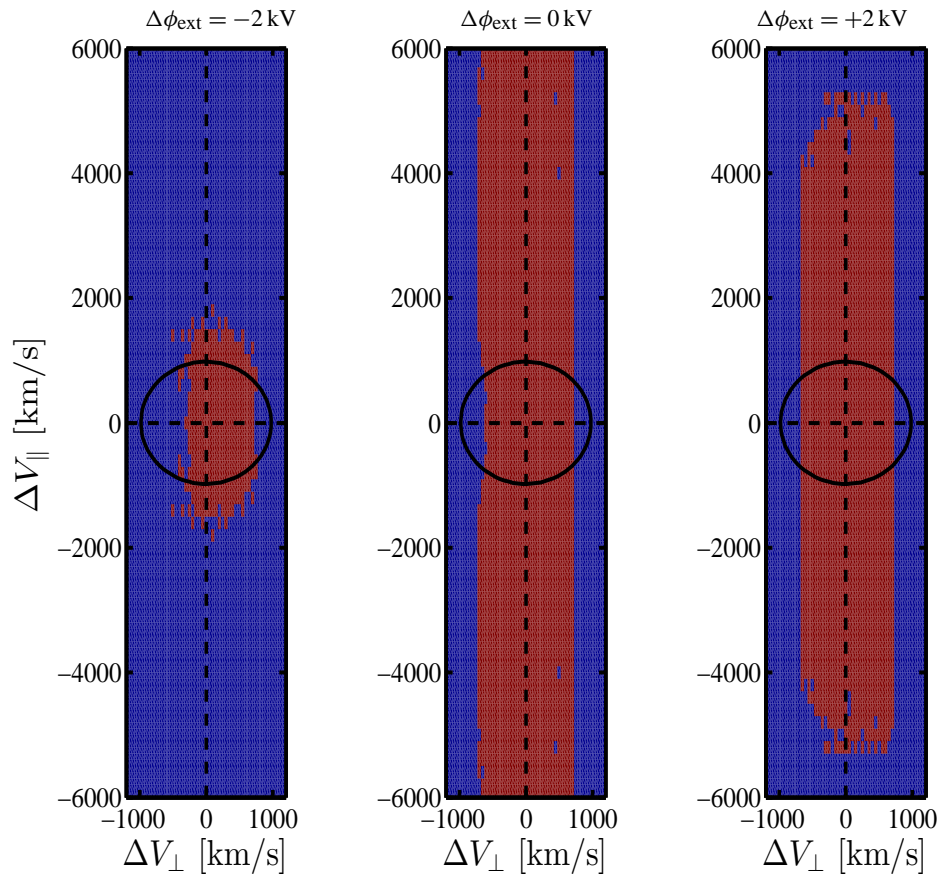


Fig. 8. Existence of a tangential discontinuity equilibrium at the cold–hot interface in the presence of both a flow shear ΔV and an EEPD $\Delta\phi_{\text{ext}} = -2\text{ kV}, 0\text{ kV},$ and $+2\text{ kV}$ for $\ell = 1$. The red regions indicate the existence of a tangential discontinuity; in the blue regions no tangential discontinuity equilibrium is possible. The circles, drawn at $\Delta V = \ell v_{\text{hot}+} = 979\text{ km s}^{-1}$, are indicative of the regions where flow shear driven instabilities might develop.

This reasoning again does not address instability issues. In general, it is known that flow shear driven instabilities appear when the velocity difference is larger than the thermal velocities and when the shear layer becomes narrower. The regions outside the circles in Fig. 8 qualitatively represent situations prone to such instabilities; the circles are drawn at $\Delta V = \ell v_{\text{hot}+} = 979\text{ km s}^{-1}$.

8 Conclusions

The present systematic study of tangential discontinuity structure, computed with a self-consistent kinetic model, elaborates on the results reported by De Keyser et al. (2010). It shows that a strong external electric potential difference invariably leads to monopolar electric field signatures at both cold–hot and hot–hot interfaces, whereas for smaller EEPD the electric field profile is monopolar or asymmetrically bipolar for cold–hot interfaces, and bipolar or more complicated for interfaces between plasmas with comparable temperatures. Parameter surveys of the solutions have been con-

ducted, demonstrating that this is a robust conclusion, regardless of the precise plasma densities or temperatures involved. Significant plasma shear flow can be important in addition to the EEPD: there is both a maximum to the EEPD and to the magnitude of the flow shear that can be sustained in an equilibrium tangential discontinuity configuration.

This finding has important implications for the generators of quasi-static auroral and subauroral features. Cold–hot plasma interfaces are found, for instance, between the lobe and the plasma sheet. Since auroral field lines connecting to the plasma sheet are likely closed, while the lobe field lines may be open, an important EEPD may exist across such interfaces. According to the TD model, such interfaces are characterized by essentially monopolar electric fields, which explains the observational results (Johansson et al., 2006; De Keyser et al., 2011). Cold–hot plasma interfaces are also found at the edges of hot plasma regions that are embedded in the lobe plasma, and that have been associated with polar cap arcs (Maggiolo et al., 2011; De Keyser et al., 2010). Yet another situation where hot and cold plasmas are

in contact occurs at the inner plasma sheet–plasma trough interface, or at the ring current–plasmasphere interface during hot plasma injection into the inner magnetosphere in the course of a substorm. Shear flow across such interfaces, rather than an EEPD, appears to provide a more appropriate description of such configurations, which may give rise to the very strong monopolar magnetospheric and ionospheric electric fields driving subauroral polarization streams or subauroral ion drift layers (De Keyser, 1999; De Keyser and Echim, 2010). Also the low latitude boundary layer can be an interface between cold plasma of solar wind origin and hot magnetospheric plasma. In that case both EEPD and flow shear may be important; the role of flow shear and its consequences for the coupling to the ionosphere has been studied by Echim et al. (2008). Hot–hot interfaces, on the contrary, are found within the plasma sheet and are associated with bipolar or more complicated electric fields for small EEPD and with monopolar signatures for large EEPD, where “small” and “large” are relative to the energy of the hottest population involved, which also appears to be compatible with observations (Johansson et al., 2006).

The TD model states that the length scales inherent in the generator electric field are set by the ion and electron gyroradii, which cover a broad range of scales. In addition, studies of quasi-static auroral current circuits associated with monopolar and bipolar electric fields indicate that the auroral signatures can involve an even broader set of length scales, depending on the interplay between the generator length scales, the ionospheric conductivity and the strength of the field-aligned currents (De Keyser et al., 2010). This may explain at least part of the wide length scale spectrum observed in auroral structures (see, e.g. Knudsen et al., 2001), although other processes must be at work as well, especially for the smallest scales (Borovsky, 1993).

There clearly are physical limits to the maximum EEPD that can be supported by an interface. The TD model is able to describe this quantitatively. But even if the interface was not exactly a TD, or if it was not planar, such limits must still exist and they must be compatible with the planar TD results. The presence of such limits imposes major constraints on the set of possible magnetospheric equilibrium configurations. In particular, the intensification of electric potential differences across the magnetotail due to enhanced solar wind–magnetosphere coupling may disrupt existing interfaces and lead to a rearrangement of the plasma. The appearance of fast magnetospheric flows may have a similar effect. In either case, the electric field variations inside the layer become larger, possibly triggering instabilities that may smoothen those variations by widening the structures. Indeed, if the length scales increase, the TD equilibrium is stable up to larger EEPD. Alternatively, a single discontinuity may break up in multiple layers, which together can support larger EEPD. The findings presented in this paper therefore highlight the need for more detailed study of the electric potential distribution and plasma flows in the magnetotail.

The TD model describes the generator of the auroral current system in the limit where no current is drawn. For quasi-static auroral structures, with their relatively long lifetime, such a description is appropriate. The model presented here thus does not include any parallel currents; such currents would modify the magnetic field (but that perturbation is known to be small). Precipitation and the presence of upward accelerated electrons or ionospheric H^+ and O^+ outflows are believed to have minor effects on the actual TD structure. To obtain a complete picture of the auroral circuit, the model should be extended self-consistently with a description of the parallel currents and of the ionospheric conductivity. Doing so is unlikely to modify the TD existence limits dramatically.

Acknowledgements. This work was supported by the Belgian Science Policy Office through Prodex-CLUSTER PEA4200090316 and Action project MO/35/031.

Topical Editor L. Blomberg thanks A. Vaivads and one anonymous referee for their help in evaluating this paper.

References

- Angelopoulos, V., Baumjohann, W., Kennel, C. F., Coroniti, F. V., Kivelson, M. G., Pellat, R., Walker, R. J., Lühr, H., and Paschmann, G.: Bursty bulk flows in the inner central plasma sheet, *J. Geophys. Res.*, 97, 4027–4039, 1992.
- Borovsky, J. E.: Auroral arc thicknesses as predicted by various theories, *J. Geophys. Res.*, 98, 6101–6138, 1993.
- De Keyser, J.: Formation and evolution of subauroral ion drifts in the course of a substorm, *J. Geophys. Res.*, 104, 12339–12350, 1999.
- De Keyser, J. and Echim, M.: Auroral and sub-auroral phenomena: an electrostatic picture, *Ann. Geophys.*, 28, 633–650, doi:10.5194/angeo-28-633-2010, 2010.
- De Keyser, J., Roth, M., Lemaire, J., Tsurutani, B., Ho, C., and Hammond, C.: Theoretical plasma distributions consistent with Ulysses magnetic field observations in a high-speed solar wind tangential discontinuity, *Solar Phys.*, 166, 415–422, 1996.
- De Keyser, J., Roth, M., Tsurutani, B., Ho, C., and Phillips, J.: Solar wind velocity jumps across tangential discontinuities: Ulysses observations and kinetic interpretation, *A&A*, 321, 945–959, 1997.
- De Keyser, J., Maggiolo, R., and Echim, M.: Monopolar and bipolar auroral electric fields and their effects, *Ann. Geophys.*, 28, 2027–2046, doi:10.5194/angeo-28-2027-2010, 2010.
- De Keyser, J., Maggiolo, R., Echim, M., and Dandouras, I.: Wave signatures and electrostatic phenomena above aurora: Cluster observations and modeling, *J. Geophys. Res.*, 116, A06224, doi:10.1029/2010JA016004, 2011.
- Echim, M. M., Roth, M., and De Keyser, J.: Sheared magnetospheric plasma flows and discrete auroral arcs: a quasi-static coupling model, *Ann. Geophys.*, 25, 317–330, doi:10.5194/angeo-25-317-2007, 2007.
- Echim, M. M., Roth, M., and De Keyser, J.: Ionospheric feedback effects on the quasi-stationary coupling between LLBL and post-noon/evening discrete auroral arcs, *Ann. Geophys.*, 26, 913–928, doi:10.5194/angeo-26-913-2008, 2008.

- Echim, M. M., Maggiolo, R., Roth, M., and De Keyser, J.: A magnetospheric generator driving ion and electron acceleration and electric currents in a discrete auroral arc observed by Cluster and DMSP, *Geophys. Res. Lett.*, 36, L12111, doi:10.1029/2009GL038343, 2009.
- Echim, M., Maggiolo, R., De Keyser, J., Zhang, T. L., Voiccu, G., Barabash, S., and Lundin, R.: Comparative investigation of the Terrestrial and Venusian magnetopause: kinetic modeling and experimental observations by Cluster and Venus Express, *Planet. Space Sci.*, 59, 1028–1038, doi:10.1016/j.pss.2010.04.019, 2011.
- Engwall, E., Eriksson, A. I., André, M., Dandouras, I., Paschmann, G., Quinn, J., and Torkar, K.: Low-energy (order 10 eV) ion flow in the magnetotail lobes inferred from spacecraft wake observations, *Geophys. Res. Lett.*, 33, L06110, doi:10.1029/2005GL025179, 2006.
- Haaland, S., Paschmann, G., Förster, M., Quinn, J., Torbert, R., Vaith, H., Puhl-Quinn, P., and Kletzing, C.: Plasma convection in the magnetotail lobes: statistical results from Cluster EDI measurements, *Ann. Geophys.*, 26, 2371–2382, doi:10.5194/angeo-26-2371-2008, 2008.
- Hubert, D., Harvey, C., Roth, M., and De Keyser, J.: Electron density at the subsolar magnetopause for high magnetic shear: ISEE 1 and 2 observations, *J. Geophys. Res.*, 103, 6685–6692, 1998.
- Johansson, T., Karlsson, T., Marklund, G., Figueiredo, S., Lindqvist, P.-A., and Buchert, S.: A statistical study of intense electric fields at 4–7 R_E geocentric distance using Cluster, *Ann. Geophys.*, 23, 2579–2588, doi:10.5194/angeo-23-2579-2005, 2005.
- Johansson, T., Marklund, G., Karlsson, T., Liléo, S., Lindqvist, P.-A., Marchaudon, A., Nilsson, H., and Fazakerley, A.: On the profile of intense high-altitude auroral electric fields at magnetospheric boundaries, *Ann. Geophys.*, 24, 1713–1723, doi:10.5194/angeo-24-1713-2006, 2006.
- Knudsen, D. J., Donovan, E. F., L., C. L., Jackel, B., and Shaw, W. D.: Width and structure of mesoscale optical auroral arcs, *Geophys. Res. Lett.*, 28, 705–708, 2001.
- Lee, L. C. and Kan, J. R.: A unified kinetic model of the tangential magnetopause structure, *J. Geophys. Res.*, 84, 6417–6426, doi:10.1029/JA084iA11p06417, 1979.
- Lemaire, J. and Burlaga, L. F.: Diamagnetic boundary layers: a kinetic model, *Astrophys. and Space Sci.*, 45, 303–325, 1976.
- Lyons, L. R.: Generation of large-scale regions of auroral currents, electric potentials and precipitation by the divergence of the convection electric field, *J. Geophys. Res.*, 85, 17–24, 1980.
- Lyons, L. R.: Discrete aurora as the direct result of an inferred high altitude generating potential distribution, *J. Geophys. Res.*, 86, 1–8, 1981.
- Maggiolo, R., Echim, M., De Keyser, J., Fontaine, D., Jacquy, C., and Dandouras, I.: Polar cap ion beams during periods of northward IMF: Cluster statistical results, *Ann. Geophys.*, 29, 771–787, doi:10.5194/angeo-29-771-2011, 2011.
- Roth, M., Evans, D. S., and Lemaire, J.: Theoretical structure of a magnetospheric plasma boundary: Application to the formation of discrete auroral arcs, *J. Geophys. Res.*, 98, 11411–11423, 1993.
- Roth, M., De Keyser, J., and Kuznetsova, M. M.: Vlasov theory of the equilibrium structure of tangential discontinuities in space plasmas, *Space Sci. Rev.*, 76, 251–317, 1996.
- Sestero, A.: Structure of plasma sheaths, *Phys. Fluids*, 7, 44–51, 1964.
- Sestero, A.: Vlasov equation study of plasma motion across magnetic fields, *Phys. Fluids*, 9, 2006–2013, 1966.
- Whipple, E. C., Hill, J. R., and Nichols, J. D.: Magnetopause structure and the question of particle accessibility, *J. Geophys. Res.*, 89, 1508–1516, doi:10.1029/JA089iA03p01508, 1984.